Laparoscopic Surgical Robot for Remote *In Vivo* Training

Brian Allen[a*] Brett Jordan[b] William Pannell[b] Catherine Lewis[c]

Erik Dutson[c] Petros Faloutsos[a]

[a] Department of Computer Science, University of California at Los Angeles, 4732 Boelter Hall, Los Angeles, 90095, USA

[b] Department of Mechanical Engineering, University of California at Los Angeles, 48-121 Engineering IV, 420 Westwood Plaza, Los Angeles, 90095, USA

[c] Department of Surgery, University of California at Los Angeles, 200 UCLA Medical Plaza, Los Angeles, CA, 90095, USA

Abstract

The Laparobot is a tele-operated robot designed specifically for training surgeons in advanced laparoscopic techniques. The Laparobot allows a student to practice surgery on a remotely located animal. The system uses standard laparoscopic tools for both the student's control interface and for performing the *in vivo* surgery, thereby providing a realistic training platform for non-robotic laparoscopic surgery. By allowing students to practice surgery remotely, animal models become more accessible and less expensive, and can replace learning on human patients. The Laparobot addresses problems inherent in designing a low-cost, tele-operated robot.

keywords: laparoscopic surgery, tele-operation, animal model, surgical training

1 Introduction

Minimally invasive surgery (MIS) provides significant benefits to patients, including shorter hospital stays, smaller scars and faster healing. However, MIS procedures can be significantly more complex than their open counterparts and so require additional training. Studies of laparoscopic surgery learning show that the rate of technical complications only stabilize after 80 to 100 procedures [1, 2], and decrease with experience by as much as 50% [3].

The training and assessment problem for laparoscopic surgery is both acute and well-recognized [4]. Previous studies have shown that low-level, psychomotor skills can be taught using simple, inanimate training systems ("box trainers"), such as those from the common Fundamentals of Laparoscopic

[*] To whom correspondence should be addressed. E-mail: vector@cs.ucla.edu

Surgery (FLS) program [5]. To train higher-level skills, simplistic models may be insufficient [6]. Two main approaches for the instruction of higher-level skills are virtual reality (VR) simulators and *in vivo* animal models. While VR simulators show great promise, and may someday provide sufficient realism to make the use of living tissue in training redundant, accurate and real-time simulation of the complex deformations, piercing, tearing and cutting of organic tissue remains an unsolved problem [7].

The porcine model was recognized early-on as effective for the training of a variety of laparoscopic procedures [8, 9, 10]. Although the porcine model is a powerful pedagogical tool, there remain barriers to their widespread use in surgical training. While ethical questions about the use of animals for training are not to be ignored, generally the most limiting impediment to the use of animal models is the expense and difficulty of maintaining a veterinary facility [11]. Such expense is compounded by the need to maintain close proximity to a medical school. While possible for large and well-endowed research institutions, schools in urban areas or those with smaller numbers of students are often unable to provide animal models for training [12]. We propose a tele-operated surgical robot to alleviate this problem. Our system, the Laparobot (shown in figure 1), capitalizes on the wide availability of Internet access for data communication to allow students of surgery an inexpensive means to access animals arbitrarily distant. Using our system, schools without local access to animal facilities can partner with institutions that do have such facilities to offer training with porcine models.

Our approach builds on a long history of robotic teleoperation for laparoscopic surgery [13, 14, 15, 16, 17]. However, to date, little attention has focused on the potential for tele-operated training and the corresponding need for low-cost operating stations. Existing commercial systems for non-remote robotic surgery such as the da Vinci system (Intuitive Surgical, Inc., Mountain View, CA), are prohibitively expensive for teaching purposes. Clearly, a requirement to operate on humans, with the safeguards, tolerances and FDA-approval implied, incurs significant design and engineering constraints to ensure the safety of the patient and the reliability of the system. The goals of this project differ. Specifically, the primary driver is to provide a system with low deployment cost and overhead, sufficient ease of use, and a method of operation that precisely mirrors the motions used in laparoscopic surgery. That is, the design of this system allows remote surgery using existing, standard laparoscopic instruments and established laparoscopic procedures. Most previous robotic surgery systems designed for tele-operation, such as the BlueDRAGON [18], da Vinci [19] and Zeus [16], attempt to improve the precision, dexterity or stability of the surgeon's motions [20]. Although such improvements are useful for the primary goal of conducting surgery, they severely limit the utility as a training platform for conventional, non-robotic laparoscopic surgery. By using standard laparoscopic instruments as both the robotic manipulators and control interfaces, our approach attempts to remain transparent; to be neither beneficial to the surgeon nor a hinderance.

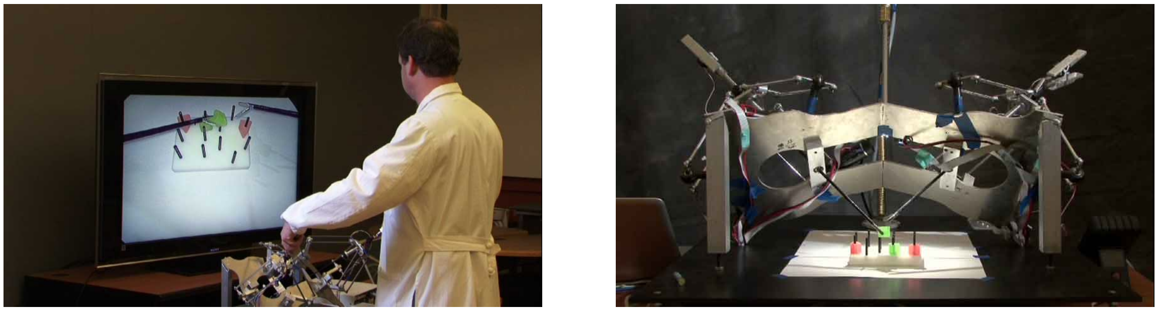

(a) The control station allows a surgeon to tele-operate using standard laparoscopic instruments in a conventional arrangement.

(b) The robot is remotely operated to perform the training task.

Figure 1: A surgeon practices a common laparoscopic training task (peg transfer) by remote operation of the robot.

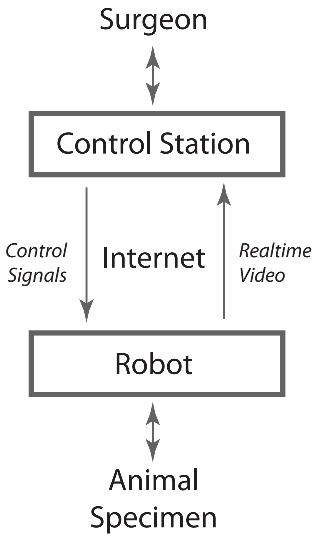

Figure 2: The flow of interaction and data through the system. The surgeon uses the system to operate on a living animal specimen at a remote location.

2 System Operation and Overview

The Laparobot functions as a human-in-the-loop tele-operated robot and is composed of two similar stations, the control station 1(a) and the surgical robot 1(b). Figure 2 illustrates the interactions of the major components. A small set of sensors tracks motions of the laparoscopic instruments manipulated by the surgeon at the control station. These motions are encoded and sent over an Internet connection to the surgical robot. The robot receives the motions as commands, and actuates its attached laparoscopic instruments to perform identically. There is a consistent one-to-one mapping of motion between the surgeon's control station instruments' motions and the surgical robot instruments' motions.

3 Surgical Robot

The surgical robot is designed to manipulate standard laparoscopic surgical tools that have a shaft diameter of 5mm and shaft length of approximately 36cm. Each instrument has five controlled degrees of freedom driven by three actuating mechanisms: positional control using a parallel mechanism (3 DOF), servo-controlled axial rotation (1 DOF), and servo-controlled grasping (1 DOF).

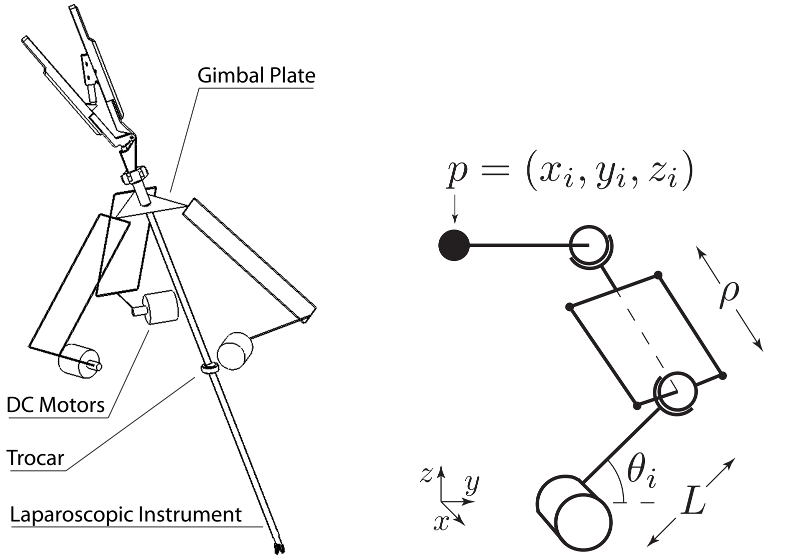

(a) Schematic view of the actuators and linkages needed to control position of one laparoscopic instrument.

(b) Diagram of the dimensions of the parallel mechanism.

Figure 3: A parallel mechanism driven by three motors is used to control the position of the laparoscopic instrument.

3.1 Positional Control using a Parallel Mechanism

The position of each laparoscopic instrument is controlled using three DC motors (Maxon 268212) interconnected by a parallel linkage based on the Delta robot [21]. The Delta mechanism rigidly affixes the positioning motors to the stationary base platform. This provides two main benefits over single-parallelogram designs, such as used in the da Vinci robot [19] and others. First, the mass of the linkages is significantly reduced, since no positioning motors need to be mounted on actuated linkages. Second, heavier and larger motors can be used for positioning, if needed, without significant alteration to the design.

However, the tight coupling of the degrees of freedom in the delta mechanism complicates the control of the robot. For example, to move the end-effector along a linear trajectory, the three motors must apply a non-linear and changing combination of torques. The approach used by the robot is an independent proportional-integral-derivative (PID) controller for each degree of freedom. That is, torque τ applied at each motor at time t is calculated as,

$$\tau(t) = k_p(\hat{\theta} - \theta) + k_i S\left(\int_{t'}^{t} \hat{\theta}(x) - \theta(x) dx\right) + k_d \frac{d\theta}{dt}, \tag{1}$$

where k_p, k_i and k_d are constants, $\hat{\theta}$ is the target position, t' is the time $\hat{\theta}$ was last changed and x is a variable of integration. $S(\cdot)$ is a saturation function limiting the "wind-up" of the integral term to the range $[-l, l]$. This function is useful in cases where the target position is unattainable, such as when blocked by collision. By limiting the range of the integral term, eventual recovery is always possible. The closed-loop control is updated at a constant rate of approximately 2000 Hz.

3.1.1 Inverse Kinematics

The PID control of equation 1 is applied in terms of the shoulder joint θ_i for the purpose of determining motor torques. Control commands received by the robot over the network specify target positions in world coordinates. Inverse kinematics maps from target position (x, y, z) to target motor angles $(\theta_1, \theta_2, \theta_2)$. Each arm of the robot is considered separately, as the motor angles are fully and independently determined by a given target position. The relation determining this inverse kinematic mapping is

$$\theta_i = \frac{\pi}{2} - \tan^{-1}(x_i/y_i) - \cos^{-1}\left(\frac{L^2 + (\frac{x_i}{\sin(\tan^{-1}(x_i/y_i))})^2 - (\rho\cos(\sin^{-1}(z_i/\rho)))^2}{2L\frac{x_i}{\sin(\tan^{-1}(x_i/y_i))}}\right) \tag{2}$$

where L and ρ are the lengths of the lower and upper arm, respectively, and θ is the motor angle. The nomenclature is shown in figure 3(b). The subscript i indicates the arm (1,2, or 3) considered.

3.1.2 Data-Driven Compensation of Static and Quasi-Static Forces

As described in the introduction, an important practical goal of the system is to support the modularity of standard commercial instruments by allowing the use of new instruments. Previously unseen instruments can be used with the system, but require an active measurement procedure to determine their mass and interaction properties.

In particular, the two main external forces being applied to the instrument are gravity and the deformation of the abdominal wall at the trocar entry point. Although in this report the trocar used has very little deformation and low friction, *in vivo* the trocar deforms the abdominal wall with each change in position. To avoid the difficult modeling problem required to predict the resulting forces on the trocar from the specimen, our system measures the actual forces, stores the data in a time-efficient data structure, and then alters the control parameters based on interpolated results of the run-time look-up.

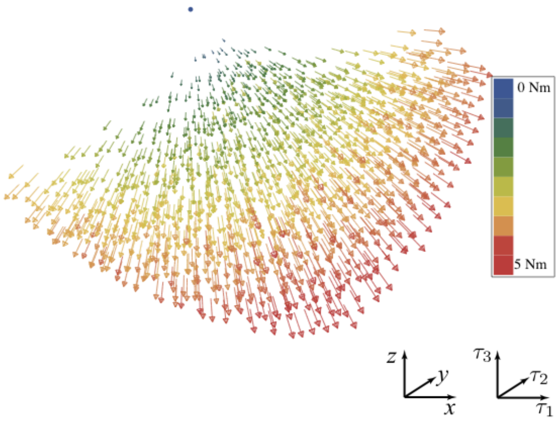

Figure 4: Visualization of the gravity-compensation torques applied at 1200 points in the workspace.

An illustrative subset of the data gathered in this process for the needle-driver instrument is represented as a vector field in figure 4. The base position of each vector is the target tool-tip position in world space. The components of each vector are the torque of each motor (τ_1, τ_2, τ_3) for that base target position. The vector's color is proportional to its length and thus denotes the total torque applied. Note that the direction and magnitude of the vector are in units of torque, while the location of the base of the vector is the target position (x, y, z). Next we describe the measurement procedure, and follow with a detailed explanation of the run-time interpolation.

The active measurement procedure is fully automated in software and requires no operator intervention. First, the magnetic position sensor described in section 4.1 is affixed to the gimbal plate of the robot, in a manner identical to that described for the control interface. A uniform grid of positions is then defined to cover the full workspace. Each grid location is targeted by the robot. Once the target is reached and the measured position is verified by the magnetic position sensor, the torques required by each motor are recorded along with the position. The target is then moved to the next grid location.

In order to minimize the time required by the procedure, target positions are chosen so that between two subsequent positions only one motor is required to change angle, and only moves by one grid position. This allows full coverage of the workspace with the minimum possible total change in motor angles. As an illustrative example, consider a three-position, three-value pattern: $(0, 0, 0)$ $(1, 0, 0)$ $(2, 0, 0)$ $(2, 1, 0)$ $(1, 1, 0)$ $(0, 1, 0)$.... Such patterns are multiple-value n-ary grey codes [22], a more complex form of the patterns used in optical encoders. While not strictly necessary, using such a pattern for active measurement significantly decreases the time and energy required for accurate torque measurements.

The resulting torque and position measurements are then stored in a three-dimensional k-d tree data structure [23]. At runtime, the k-d tree allows rapid retrieval of the torque measurements previously made in the neighborhood of a given target position. These previous measurements are then used to estimate the motor torque $\hat{\tau}$ needed at the target position. Specifically, the k nearest points $(p^1, ...p^k)$ to the target position $\hat{p}$ are found by searching the k-d tree, an operation that takes $O(n^{1-\frac{1}{3}} + k)$, where n is the total number of measurements in the data structure. Once the nearby points are identified, the corresponding sample torques $(\tau^1, ..., \tau^k)$ are retrieved, where the super-script indicates the corresponding position. Thus the torque estimate $\hat{\tau}$ for position $\hat{p}$ is

$$\hat{\tau} = \sum_{i=1}^{k} \frac{\tau^i}{k} \frac{|p^i - \hat{p}|}{\sum_{j=1}^{k} |p^j - \hat{p}|}. \tag{3}$$

To make use of the estimated torque $\hat{\tau}$ in conjunction with the PID controller, the integral term in equation 1 is instantaneously set to $\frac{\hat{\tau}}{k_i}$ with each new position target. That is, the integral term is artificially set to the value that, if the system were at the target position with zero velocity, would maintain equilibrium by balancing the expected net forces with the PID-computed torque. After the integral term is set, it is allowed to accumulate as usual. The key benefit to this approach is that it gives the system the ability to compensate for quasi-static forces arising from the deformation of the animal's abdominal wall. Note that PID control without this compensation would work, but would take significantly longer to reach equilibrium at the set-point.

3.2 Servo Control of Axial Rotation and Grasping

Axial rotation is controlled by a small servo (Futaba, Chiba, Japan) fixed beneath the gimbal plate of the delta mechanism. The gimbal plate does not rotate with the instrument, providing a rotational reference that otherwise travels with the motion of the instrument. The instrument is linked to the servo by a small gear fixed to the instrument shaft using a removable locking screw, allowing 180° of rotation. This range approximately matches the full comfortable range of motion used by the surgeons, although care is needed to ensure the range of motion of the servo is aligned to the instrument's proper orientation prior to use. The servo is able to drive the instrument through the full range of motion in 0.3 seconds, which was found sufficient for the relatively low angular velocities used in training. Figure 5 shows the axial mount.

The grasping servo motor (Futaba, Chiba, Japan) is mounted in the handle of the instrument, with the servo acting on a small lever-arm to open and close the tool grasper. The servo motor has an operating range of 90°, which is translated by a small lever arm to control the instrument's full range of grasping. The servo drives the grasper from fully closed to fully open in 0.2 seconds, with approximately 1.7 Kg-cm of torque.

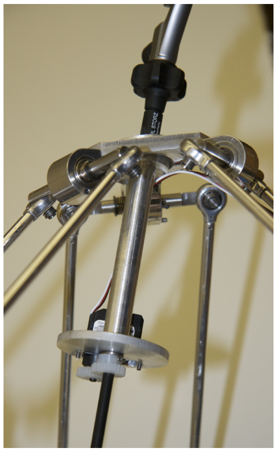

Figure 5: The axial servo is mounted on a platform attached to the center of the gimbal plate.

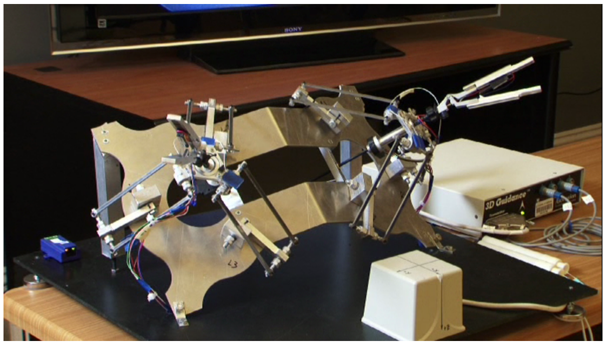

Figure 6: The control station.

4 Control Station

The control station, shown in figure 6, provides a working interface very similar to a conventional box trainer. An aluminum base-plate holds two laparoscopic instruments at a common operating angle and a non-actuated parallel kinematic linkage passively restricts the motions of the instruments to the working space of the system and thus provides a rudimentary form of proprioceptive feedback to the surgeon. The instructor interacts with the instruments as if performing a standard laparoscopic surgery while receiving visual feedback from the video monitor. By design, the ergonomic experience when controlling the robot is as close as possible to the experience of performing a procedure in the operating room. In particular, the handles are based on standard laparoscopic instruments (Karl Storz EndoscopyAmerica, Inc., Culver City, California). The instruments are modified to contain small, light-weight (4 grams) linear potentiometers (Model 9605, BEI Duncan Electronics, Irvine, California) in the handle. The potentiometer measures the grasper position (open to closed). This position is sent via the BlueTooth wireless protocol to the nearby control computer, which in turn sends the position as a control command to the robot, as described in section 5. In addition, the axial rotation of the instrument is measured by an attached optical encoder, connected to the control computer by the universal serial bus (USB).

4.1 Spatial Tracking

The instructor interfaces with the system by moving standard laparoscopic instruments. To track these motions, a small magnetic sensor (microBird from Ascension, Burlington, VT) was rigidly attached to the gimbal plate of the kinematic linkage (see section 3.2). The sensor was mounted to a small plate made of high-grade acrylic resin with a cut groove of the width of the sensor, allowing the sensor to be removed and replaced in precisely the same location relative to the gimbal plate. The sensors are small (1.3 mm) and light-weight (0.2 g) with a nominal accuracy of 0.48 mm. When stationary, the sensors report the 3D location with a precision measured to 0.13 mm of root mean square (RMS) error. This configuration was originally designed for the passive collection of motion data during training exercises [24].

5 Communication of Control Signals over the Internet

The measured state of the control station instruments is sent over a standard packet-switched Internet connection to the robot. Each of the three separate sensory systems is independent, and each uses a separate packet stream as control signal. Three control signals are sent as three separate user datagram protocol (UDP) packet streams, each on a unique and pre-assigned port. The UDP itself has neither error checking nor error correction. The computer at the control station computes a one-byte checksum on each outgoing packet to allow the receiving robot to detect corrupted packets. Corrupted, dropped and out-of-order packets are ignored. Order is determined by a millisecond time-stamp in each data packet. UDP is selected over the more complex transmission control protocol (TCP) to reduce latency and to avoid protocol-required automatic retransmission of lost or corrupted packets. Under ideal conditions the latency of both protocols is roughly equivalent for this application, however, when establishing the connection or in the case of packet loss or corruption, UDP has lower latency by up to twice the round-trip time [25].

A packet is sent as soon as a sensor detects a state-change, unless a packet was sent on that channel within the last 0.0167 seconds. In that case, a timer is set to 0.0167 seconds after the last-sent packet. On expiration of the timer, the most recent available sensor reading is encoded in a packet and sent. In this way, across all three control streams, at most $3 \times (1/0.0167) = 180$ UDP packets per second will be sent across the network per instrument. Using three separate streams allows three separate timers, reducing the latency, since packets are sent on detected changes in state. The position control packets carry three positions of four bytes each, plus the common four-byte timestamp. Both axial and grasper control packets hold a single four-byte value in addition to the timestamp. The UDP format requires eight bytes, and IPv4 an additional 20. Using the standard configuration with two instruments controlled, the maximum data rate used is 13920 bytes/second, or less than 140 kbps. Network delays beyond transmission time are not modeled and may result in unexpected lag to the system. However, in practice, the risk of such delays can be mitigated by using dedicated transmission lines.

5.1 Laparoscopic Video Feedback

Whereas the control signals travel from the the control station to the robot, a live video stream is captured at the robot and sent to the control station. The video camera is a Storz Endoskope (Karl Storz EndoscopyAmerica, Inc., Culver City, California) providing a resolution of 768 by 494 pixels. The video signal is encoded and transmitted to the control station. When a closed-circuit video connection is not available, the video is encoded to H.264 (MPEG-4 Part 10) at 24 fps with an encoding latency of approximately 30 ms. The resulting video stream requires approximately 2 Mbps.

6 Results

To objectively evaluate the performance of the system, the positional and tracking accuracies are measured. While there are a number of surgical systems designed for human operations, to our knowledge, no tele-operated *in vivo* training robots have been described previously.

6.1 Measured Accuracy

Accuracy is paramount to successful tele-operational surgery. Positional error can occur in both the positional sensing and the robotic control. Sensory accuracy is described and quantified in Section 4. In this section, measurement of the accuracy of the robot and control system is reported.

As described in section 4.1, the observed RMS error in spatial tracking was 0.13 mm. For validation experiments, a second magnetic sensor was affixed to the distal tip of the instrument. This distal sensor is necessarily less precise due to magnetic field interference caused by the mounting hardware and motors in the vicinity of the magnetic emitter and the sensor. The observed RMS error for this distal sensor was 0.25 mm, approximately twice the observed error in the handle sensor.

To measure tracking accuracy, a trajectory is generated analytically and sampled at 15 Hz. Each sample is sent over the network as a stream of control packets in a manner indistinguishable from motions generated by the surgeon's control console.

During testing, a magnetic sensor, equivalent to those used by the surgeon control console and described in section 4.1, is rigidly fastened to the tool-tip of the instrument. This setup allows precise tracking of the instrument in the same coordinate system that motion commands are specified. Before each test, the position of the instrument is calibrated to eliminate static positional error.

Two types of measurements were collected, the motion trajectory resulting from a discrete change in the target position (point-to-point), and the error in position while dynamically tracking a linear trajectory. Figure 7 shows the (X,Y,Z) position of the tool-tip in the world coordinate frame. The target position is changed every ten seconds to a point 22.1 mm away. The overshoot in position ranges

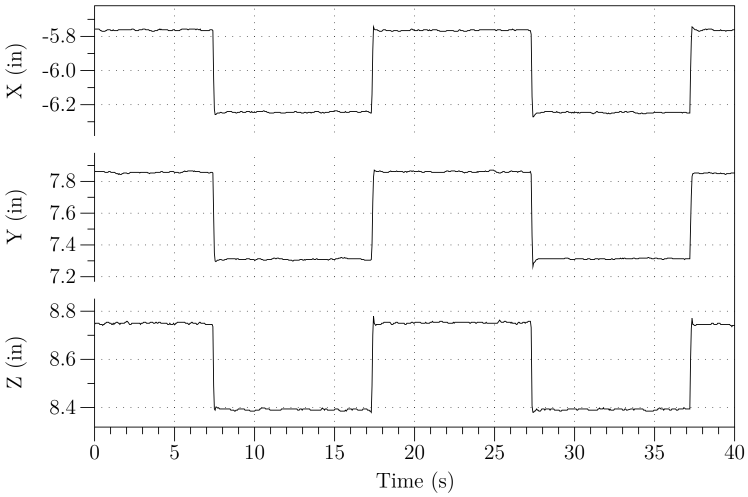

Figure 7: Trajectory in X, Y and Z planes while targeting a set-point that changes position by 22.1 mm every ten seconds.

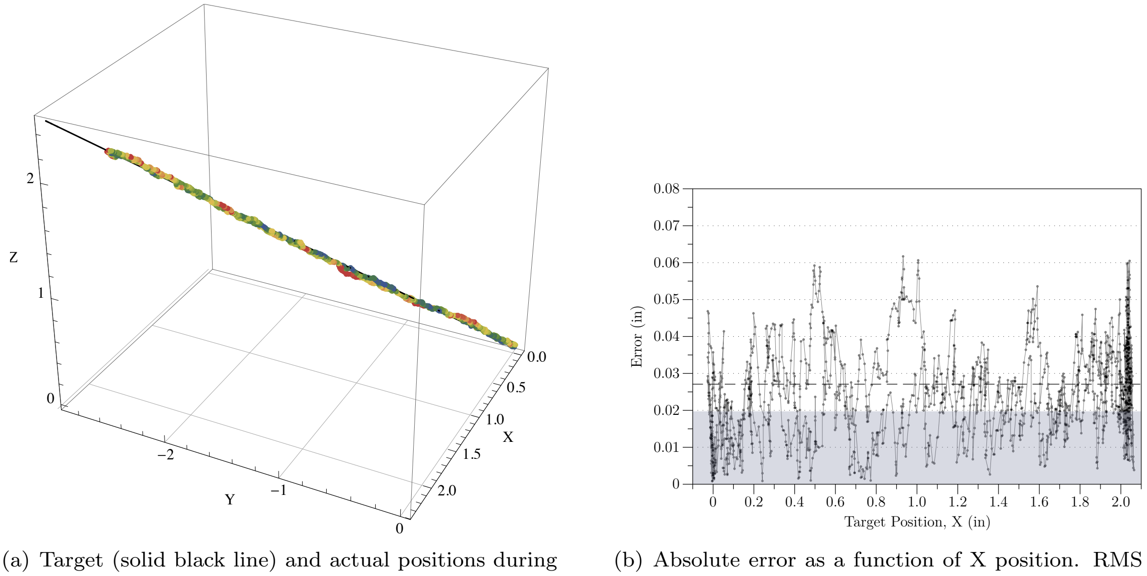

(a) Target (solid black line) and actual positions during tracking. Color indicates the amount of error for that sample, with red points being the locations of highest error.

(b) Absolute error as a function of X position. RMS of the error indicated by the bold dashed horizontal line.

Figure 8: Sampled error while tracking of a linear trajectory at 10.2 mm/sec.

between a maximum of 0.89 mm to less than the RMS error of the position sensor (0.13 mm). The noise in the position between changes in position is due to noise in the position sensor.

The second type of collected measurement is linear tracking. Note that tracking a world-space line requires motion from all three motors and is a test of motor coordination, rather than a single degree of freedom. Figure 8 reports the actual trajectory followed by the tool-tip during a 10.2 mm/sec linear motion and the observed error from target trajectory during that motion. The RMS of the error is shown as a horizontal dashed line, along with a grey band indicating the nominal precision of the position measurement.

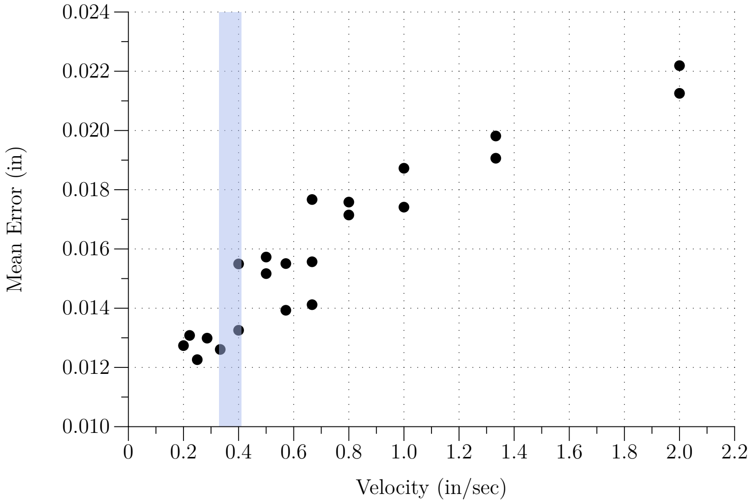

Figure 9: Linear trajectory error as a function of target velocity. The shaded band indicates measured mean velocities during training tasks.

The target trajectory of figure 8 has a velocity of 10.2 mm/sec. This was experimentally found to be the mean velocity when expert surgeons performed a basic training task (peg transfer). Other tested tasks, such as passing a rope and capping a needle, had lower mean velocities (see [24] for details on collection procedures). As the velocity of the target position increases, the mean observed error also increases. This relationship is shown in figure 9. The shaded vertical line shows the range of mean velocities observed during expert performance of training tasks.

6.2 Workspace

The workspace of the robot is the region of space reachable by the tool-tip of the laparoscopic instrument. The workspace must be sufficiently large to allow unfettered motion within the abdominal cavity of the animal. A recent study [26] characterized the workspace used across seven surgical tasks in a porcine model. This report described a workspace of a solid circular cone with a vertex angle of 60° would contain 95% of tool-tip motion for the porcine model. The workspace of the mechanism proposed here provides a maximum lateral range of 65° and a maximum anteroposterior angle of 72°. This workspace has a complex shape due to the geometric complexity of the parallel mechanism. The workspace of the robot is shown in figure 10.

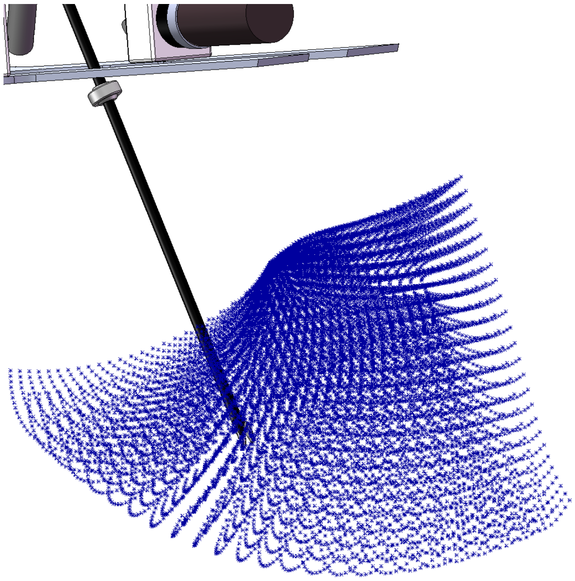

Figure 10: Blue sample points illustrate the working space of the tool-tip.

7 Conclusion

The training of laparoscopic surgeons has been and remains an important topic of research for nearly twenty years. It is widely recognized that animal models provide an excellent basis for learning advanced surgical skills. Although greater use of animals for training has significant ethical questions, those questions are matched by the significant differences in error rate and post-surgery complication rate between new surgeons and experienced surgeons. Training based on animal models may reduce the risk associated with a surgeon's early-career procedures. At the present time, however, few surgeons are provided the opportunity to train using porcine models due to the expense and remoteness of animal facilities.

Tele-robotics may provide a solution. The proposed Laparobot aims to complement the final stages of a surgeon's education with *in vivo* training, and thereby to reduce the number of complications arising during a surgeon's first procedures. Future versions of the Laparobot will investigate the ability of tactile feedback, such as through a pneumatic display [27], and proprioceptive feedback, obtained by adding actuators to the control console, to improve the fidelity of the training experience.

Acknowledgments

The study was partially supported by the US Army Telemedicine and Advanced Technologies Research Center (TATRC). We wish to thank Karl Storz Endoscopy-America, Inc., Intel Corp., and Autodesk Inc. for generous support through equipment and software grants. We also wish to thank Vasile Nistor and Greg Carman for their contributions to the mechanical design, helpful advice and discussions.

REFERENCES

[1] D. J. Biau, S. M. Williams, M. M. Schlup, R. S. Nizard, and R. Porcher. Quantitative and individualized assessment of the learning curve using lc-cusum. *British Journal of Surgery*, 95(7):925–929, 2008.

[2] T Sovik, E T Aasheim, J Kristinsson, CF Schou, L My Diep, A Nesbakken, and T Mala. Establishing laparoscopic roux-en-y gastric bypass: Perioperative outcome and characteristics of the learning curve. *Obesity Surgery*, 19(2):158–165, 2009.

[3] P. Schauer, S. Ikramuddin, G. Hamad, and W. Gourash. The learning curve for laparoscopic roux-en-y gastric bypass is 100 cases. *Surgical Endoscopy*, 17(2):212–215, February 2003.

[4] R. Aggarwal, K. Moorthy, and A. Darzi. Laparoscopic skills training and assessment. *British Journal of Surgery*, 91(12):1549–1558, 2004.

[5] J.H. Peters, G.M. Fried, L.L. Swanstrom, N.J. Soper, L.F. Sillin, B. Schirmer, and K. Hoffman. Development and validation of a comprehensive program of education and assessment of the basic fundamentals of laparoscopic surgery. *Surgery*, 135(1):21–27, 2004.

[6] J.U. Stolzenburg, M.C. Truss, R. Rabenalt, M. Do, T. Schwalenberg, P.F. Katsakiori, A. McNeill, and E. Liatsikos. Training in Laparoscopy. *EAU-EBU Update Series*, 5(2):53–62, 2007.

[7] S. Misra, KT Ramesh, and A.M. Okamura. Modeling of tool-tissue interactions for computer-based surgical simulation: A literature review. *Presence: Teleoperators and Virtual Environments*, 17(5):463–491, 2008.

[8] W.O. Kirwan, T.K. Kaar, and R. Waldron. Starting laparoscopic cholecystectomy—The pig as a training model. *Irish Journal of Medical Science*, 160(8):243–246, 1991.

[9] DI Watson, PJ Treacy, and JAR Williams. Developing a training model for laparoscopic common bile duct surgery. *Surgical Endoscopy*, 9(10):1116–1118, October 1995.

[10] A. Olinger, G. Pistorius, W. Lindemann, B. Vollmar, U. Hildebrandt, and MD Menger. Effectiveness of a hands-on training course for laparoscopic spine surgery in a porcine model. *Surgical Endoscopy*, 13(2):118–122, February 1999.

[11] FP Gruber and T. Hartung. Alternatives to animal experimentation in basic research. *ALTEX: Alternativen zu Tierexperimenten*, 21:3–31, 2004.

[12] K.E. Roberts, R.L. Bell, and A.J. Duffy. Evolution of surgical skills training. *World Journal of Gastroenterology*, 12(20):3219–3224, May 2006.

[13] J.W. Hill, P.S. Green, J.F. Jensen, Y. Gorfu, and A.S. Shah. Telepresence surgery demonstration system. In *IEEE International Conference on Robotics and Automation*, pages 2302–2307, San Diego, CA, USA, May 1994.

[14] MC Cavusoglu, F. Tendick, M. Cohn, and SS Sastry. A laparoscopic telesurgical workstation. *IEEE Transactions on Robotics and Automation*, 15(4):728–739, 1999.

[15] A Madhani, G Niemeyer, and J Salisbury. The black falcon: a teleoperated surgical instrument for minimally invasive surgery. In *Proceedings of IEEE/RSJ International Conference on Intelligent Robots and Systems*, volume 2, pages 936–944, Victoria, Canada, October 1998.

[16] J Marescaux, J Leroy, F Rubino, M Smith, and M Vix. Transcontinental robot-assisted remote telesurgery: feasibility and potential applications. *Annals of Surgery*, 235(4):487–492, 2002.

[17] P. Berkelman and J. Ma. The University of Hawaii teleoperated robotic surgery system. In *IEEE/RSJ International Conference on Intelligent Robots and Systems*, pages 2565–2566, San Diego, CA, USA, 2007.

[18] M.J.H. Lum, D. Trimble, J. Rosen, K.F. Ii, H.H. King, G. Sankaranarayanan, J. Dosher, R. Leuschke, B. Martin-Anderson, M.N. Sinanan, et al. Multidisciplinary approach for developing a new minimally invasive surgical robotic system. In *Biomedical Robotics and Biomechatronics, 2006. BioRob 2006. The First IEEE/RAS-EMBS International Conference on*, pages 841–846, 2006.

[19] G.S. Guthart and J.K. Salisbury. The IntuitiveTM telesurgery system: overview and application. In *IEEE International Conference on Robotics and Automation*, volume 1, pages 618–621. San Francisco, CA. USA, 2000.

[20] A.R. Lanfranco, A.E. Castellanos, J.P. Desai, and W.C. Meyers. Robotic surgery: a current perspective. *Annals of Surgery*, 239(1):14, 2004.

[21] R. Clavel. Delta, a fast robot with parallel geometry. In *Proc. of the 18th International Symposium on Industrial Robots (ISIR)*, pages 91–100, Lausanne, Switzerland, 1988.

[22] P. Elias. Coding for noisy channels. *IRE Conv. Rec.*, 3(4):37–46, March 1955.

[23] J.H. Friedman, J.L. Bentley, and R.A. Finkel. An algorithm for finding best matches in logarithmic expected time. *ACM Transactions on Mathematical Software (TOMS)*, 3(3):209–226, 1977.

[24] B Allen, V Nistor, E Dutson, G Carman, C Lewis, and P Faloutsos. Support vector machines improve the accuracy of evaluation for the performance of laparoscopic training tasks. *Surgical Endoscopy*, 24(1):170–178, January 2010.

[25] J. Postel. User datagram protocol. RFC 768, Internet Engineering Task Force, August 1980.

[26] M Lum, D Trimble, J Rosen, K Fodero, H King, G Sankaranarayanan, J Dosher, R Leuschke, B Martin-Anderson, M Sinanan, and B Hannaford. Multidisciplinary approach for developing a new minimally invasive surgical robotic system. In *IEEE/RAS-EMBS International Conference on Biomedical Robotics and Biomechatronics (BioRob)*, pages 841–846, Pisa, Italy, February 2006.

[27] CH King, MO Culjat, ML Franco, JW Bisley, E. Dutson, and WS Grundfest. Optimization of a pneumatic balloon tactile display for robot-assisted surgery based on human perception. *IEEE transactions on bio-medical engineering*, 55(11):2593, 2008.